Results in Engineering 31 (2026) 111572

Contents lists available at ScienceDirect

Results in Engineering

journal homepage: www.sciencedirect.com/journal/results-in-engineering

Research paper

Design approach and performance of a scalable granular packed bed biofilter for electro-fermentation

Maximilian Miehle [a], Johannes Gescher [b], Harald Horn [a,c], Andrea Hille-Reichel [a,*]

[a] Engler-Bunte-Institut, Water Chemistry and Water Technology, Karlsruhe Institute of Technology (KIT), Engler-Bunte-Ring 9a, 76131 Karlsruhe, Germany
[b] Institute of Technical Microbiology, Hamburg University of Technology, Hamburg 21073, Germany
[c] DVGW Research Centre, Water Chemistry and Water Technology, Engler-Bunte-Ring 9a, 76131 Karlsruhe, Germany

ARTICLE INFO

Keywords:
Electro-fermentation
Microbial electrolysis cell (MEC)
Packed-bed BES reactor
Shewanella oneidensis

ABSTRACT

Bioelectrochemical systems (BES) represent a promising technology for the production of energy, energy carriers, and chemicals; however, their implementation in industrial applications faces significant challenges related to scalability. In this study, we introduce a novel, scalable, single-chamber BES in which the working electrode is realised as a packed bed of electrically conductive equal-sized spheres made from a graphite-polymer composite. The reactor has a total volume of 3.56 L and a packed bed volume of 1.66 L with an electrode surface area of 1.06 m^2. A model microbial electrolysis / electro-fermentation of lactate to acetate was catalysed by the exoelectrogenic bacterium *Shewanella oneidensis*, achieving a maximum current density of 430 mA m^{-2} at an anode potential of 300 mV relative to the standard hydrogen electrode.

1. Introduction

Anaerobic fermentation, i.e. fermentation in the absence of oxygen, is a frequently utilised and desired application in biotechnology due to cost efficiency [1]. BES systems enable oxidation reactions under anoxic circumstances by transferring emerging electrons from the reaction to the surface of an anode [2].

Therefore, the aim of all BES designs is to provide an extensive electrode surface for the attachment and biofilm formation of electroactive microorganisms. The BES should allow controlling biofilm thickness to mitigate mass transport limitations due to mostly diffusive transport of substrates into or products out of the film and to enable sufficiently high electron transfer rates between the electrode surface and microorganisms in the biofilm. These transfer rates are determined by the electron transport characteristics of the respective organism and are, among others, influenced by the spatial distance between the microorganism in the biofilm and the anode surface. The latter should exhibit no toxicity for microorganisms and hence good biocompatibility, and stand out with high conductivity to keep ohmic losses to a minimum.

BES have been designed as either dual-chamber or single-chamber systems. One critical design element of dual chamber systems is the proton exchange membrane (PEM), which is prone to fouling and intern resistance issues and therefore difficult to scale-up, as well to leaking polyfluoralkyl substances (PFAS) into the environment [3,4]. Also, in white biotechnology using biocatalyst monocultures, moist heat sterilisation is a reliable sterilisation method but not suitable for most membranes.

Single-chamber systems address these scale-up issues, on the other hand, by not using a PEM in the first place, but allowing unwanted crossover between anode and cathode reaction species, which occurs by placing the anode and cathode in the same chamber [5].

In the past, several concepts were developed for the scale-up of single chamber BES. Rader & Logan and Cusick et al., for example, both used graphite fibre brushes for their reactor design [6,7]. A drawback is the inherent difficulty to determine the active surface and hydrodynamic

Maximilian Miehle: Karlsruhe Institute of Technology (KIT), Engler-Bunte-Institut, Water Chemistry and Water Technology, Engler-Bunte-Ring 9a, 76131 Karlsruhe, Germany

Johannes Gescher: Hamburg University of Technology, Institute of Technical Microbiology, Kasernenstraße 12, Hamburg 21073, Germany

Harald Horn: Karlsruhe Institute of Technology, Engler-Bunte-Institut, Water Chemistry and Water Technology, Engler-Bunte-Ring 9, Karlsruhe 76131, Germany

* Corresponding author at:Karlsruhe Institute of Technology (KIT), Engler-Bunte-Institut, Water Chemistry and Water Technology, Engler-Bunte-Ring 9a, 76131 Karlsruhe, Germany.

E-mail addresses: maximilian.miehle@kit.edu (M. Miehle), johannes.gescher@tuhh.de (J. Gescher), harald.horn@kit.edu (H. Horn), andrea.hille-reichel@kit.edu (A. Hille-Reichel).

https://doi.org/10.1016/j.rineng.2026.111572
Received 21 April 2026; Received in revised form 2 June 2026; Accepted 14 June 2026
Available online 15 June 2026

conditions inside the graphite fibre brushes, furthermore, clogging can become an issue [8].

Rotating disc reactors as scaled-up BES (RDBER, rotating disc bioelectrochemical reactor) were designed by Hackbarth et al. [9] and used in several studies [10–12]. Shylaja Prakash et al. who investigated the 100-L version of this reactor describe mass transfer limitations due to small spatial distance between the co-rotating electrodes as a main parameter to be optimised [12].

A third concept are biofilters (packed bed reactors), which are known for their easy scalability and their application as plug flow systems for efficient substrate usage and maximum product generation [13]. Thus, biofilters are frequently used in wastewater treatment [14]. Their hydrodynamics are widely understood, and tools for scale-up are available, at least for use of spheres of equal size [15,16]. Consequently, packed bed reactors were examined for their capability as scalable BES systems. Quejigo et al. investigated packed bed reactors with graphite granules of 1 to 5 mm in diameter, with a focus on understanding the distribution of electrical potential in the bulk material. They stated that with only one connecting rod-like electrode submerged in the packed bed, the bed's polarisation was insufficient, at only 10 % [17]. Aligning with that, Jiang & Li reported that increasing the amount of submerged connecting electrodes enhances the performance. They also specified that in order to save power, the distance of the cathode to the packed bed should not exceed 2 cm [18]. Wu et al. combined the dual chamber approach with stacked packed bed filters in flat and rectangular cells with promising results, but reported potential problems with clogging effects and varying flow conditions between the cells [19].

Based on the advantages of the biofilter as BES design, in this work, this concept was used to construct a new type of single-chamber BES with polymer-graphite spheres. To address the drawbacks described above, and to make maximum use of the high working electrode surface, pressure was applied to the packed bed by polarized graphite plates below and above the bed to increase connection of the bed as well as to enhance contact conductivity between the granules. Six steel rods were submerged into the packed bed as counter electrodes (cathodes) to keep the spatial distance between working and counter electrode at a minimum. Scalability of the packed bed was further enhanced by using spherical particles of equal size to facilitate the formation of a homogeneous bed and flow profile. Potential clogging can be controlled by fluidization of the packed bed. This work provides a proof of concept, using the example of lactate to acetate conversion by *S. oneidensis* as a model process for the production of a dissolved, hypothetically value-added chemical. *S. oneidensis* is a Gram-negative, facultative anaerobic, chemo-organo-heterotrophic bacterium that can utilise a vast amount of different naturally occurring electron acceptors for its respiratory metabolism such as nitrate and thiosulfate or elemental sulfur, manganese oxides and iron oxides as well as electrodes [20,21]. It is known that under anoxic conditions and in monoculture, *S. oneidensis* only forms very thin biofilms of a few cell layers, which are significantly thinner than those of "good" biofilm formers such as *G. sulfurreducens* or mixed cultures of both [22]. The reason for this seems to be *S. oneidensis*` incapability to produce electrically conductive nanowires [23]. However, the great potential of using *S. oneidensis* lies in its genetic tractability allowing for enhancing the substrate or product spectrum or increasing performance [24]. This opens up the possibility to produce, e.g. higher-value chemicals via specifically designed metabolic pathways [25], as done, for example, by Sun et al. with the conversion of glycerol to acetoin [26]. The reactor is specifically designed for the use in white biotechnology and cultivation of pure cultures as biocatalysts with voltage being provided by a potentiostat. As the fermentation requires anaerobic conditions, the reactor is run as microbial electrolysis cell (MEC) which results in the production of hydrogen as a byproduct.

2. Material and methods

2.1. Reactor design

The core part of this prototype is a packed bed reactor with a bottom-up flow, as shown in Fig. 1a-d. The reactor has a height of 363 mm and a volume of 3.56 L, while the periphery (gas trap and tubings) has a volume of 0.2 L. The reactor was realised as a hollow cylinder made of borosilicate glass (Fig. 1a, No. 1.7), with an inner diameter of 140 mm and a height of 186 mm. The cylinder is filled with a bed of electrically conductive spheres with a diameter of 5.5 to 6 mm (Fig. 1c, No. 3.1), which serves as the working electrode. The bed had a volume of 1.66 L with a void fraction of approximately 40 %. The spheres consist of a graphite-polypropylene mixture (Whitecell Eisenhuth GmbH & Co. KG, Osterode, Germany) with more than 80 % graphite to ensure conductivity and can be considered biologically inert and non-toxic. They have a density of 1.8 g mL^{-1} and a mean roughness of 3 μm by being blasted with walnut shell particles to roughen the surface and thus facilitate the adhesion of bacteria. Laser Scanning Microscopy investigations showed that surface area was enhanced by approximately 10 % (not shown). The crushing force of one sphere is 63 ± 15 N. The packed bed was poised at a positive potential relative to the standard hydrogen electrode (SHE) to operate as an anode. The bacteria are cultivated as biofilms on the spheres and convert the substrate provided in the liquid phase streaming through the packed bed from bottom to top. Substrate is fed from the feed reservoir (Fig. 1d, No. 4.10), and product-rich liquid leaves the reactor through the siphon and can be collected product reservoir (No. 4.11). Since the electrical resistance across contact surfaces decreases with increasing normal force to the contact surface [27], the packed bed is slightly compressed by two perforated circular graphite plates below and above with 50 N, which also determine the axial expansion of the bed (Fig. 1a, Nos. 1.4 and 1.9). With 84 holes of 7 mm diameter, the area of the perforations is about one-fifth of the cylinder cross-section. The perforations allow the liquid phase to pass through. Six additional holes of 20 mm diameter in both plates provide openings for the counter electrode bundles. Feed spacers, known from membrane technology, are clamped between anodes and their support structure to prevent granules from exiting the bed (No. 1.10). The lower graphite plate is connected to a potentiostat (Fig. 1d, No. 4.3) via a titanium screw (Fig. 1a, No. 1.6). The upper graphite plate connected to a titanium rod of 20 mm diameter serves as a stamp (No. 1.14), if force is applied longitudinal to the titanium rod. Ohmic resistance between connection points below the bed (1.6) and above it (Upper end of the titanium rod, 1.14), was approximately 10 Ohm. As the rod protrudes from the top cover, the entry point is sealed by sliding through a lip seal ring (No. 1.20). With the lip seal ring serving as a slide bearing, the stamp can be used to adjust the height of the upper graphite plate and, with applied force, the pressure on the bed. If a titanium screw is used for the connection (1.13), the bed can be polarised using the stamp. As an alternative, this connection can be done with a plastic screw to isolate the anode from the titanium rod. The combined surfaces of the packed bed, calculated from mean diameter and packed bed void ratio, and the graphite anodes accessible to the liquid phase amount to 1.06 m^2. Six steel (V4A) rod bundles, each composed of 9 rods of 20 cm length and 1.5 mm diameter (Fig. 1a, No. 1.8) with a bundle diameter of roughly 16 mm, are embedded in the anodic bulk material as counter-electrodes (cathodes in this application) which are shielded from the surrounding bed by perforated hollow cylinders (No. 1.12) made of polypropylene (PP). The steel rod bundles are screwed on a steel plate (1.16), which is connected to the potentiostat via a little latch (1.17). Upper and lower ends of the glass cylinder are each guided via a flange construction (bottom: Nos. 1.3 and 1.5, top: 1.15), which is held together by screws embedded into the flanges (3.2), into a conical lid construction (bottom: 1.2, top: 1.19). The inlet and outlet (bottom: 1.1, top: 1.21) of both covers are made of stainless steel and connected to the periphery. The lower lid and the flange construction are made of PP, while the upper cover, including the outlet, is made

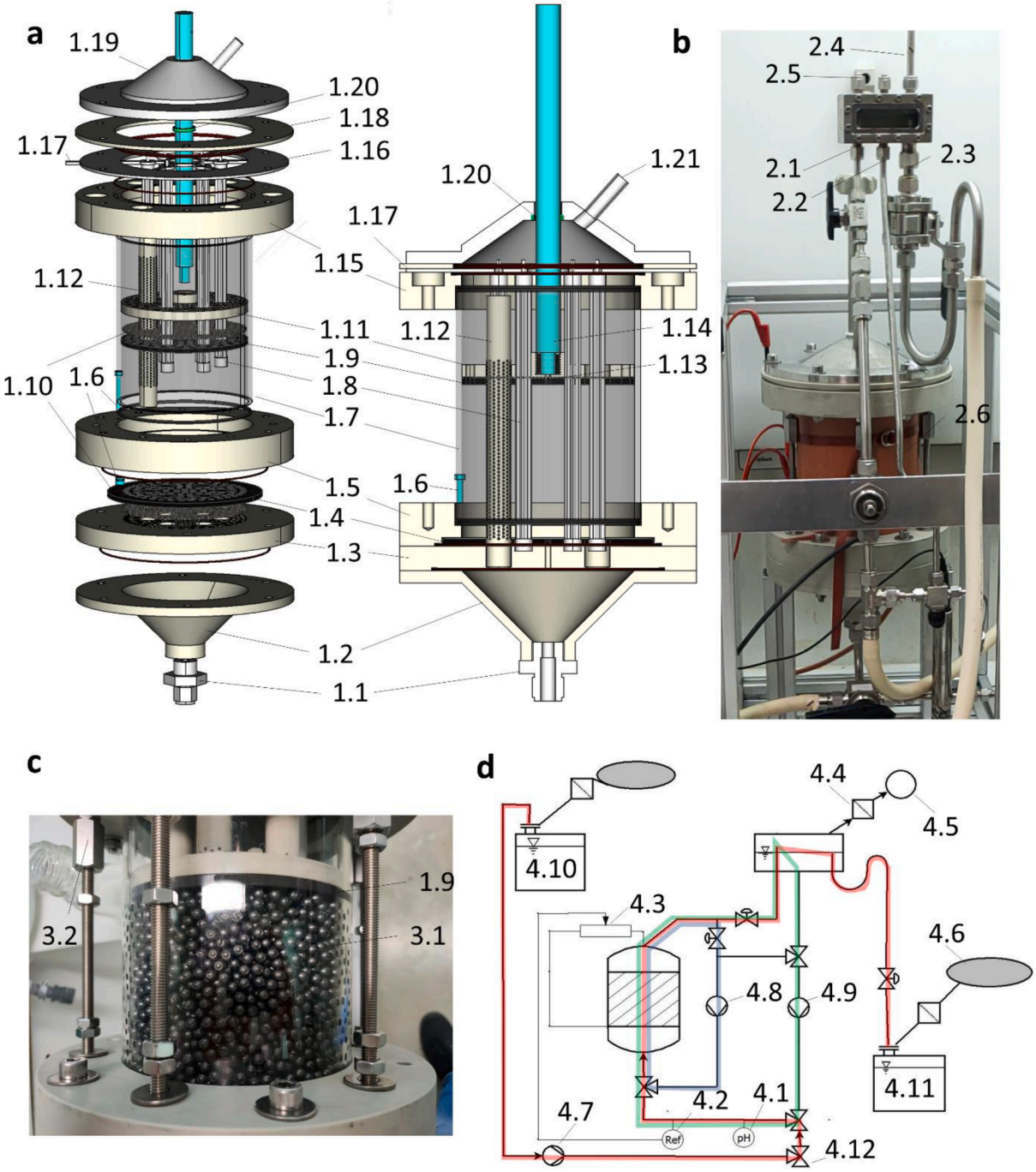

Fig. 1. a: Exploded view drawing (left) and longitudinal section (right) of the CAD model of the bioelectrochemical packed-bed reactor /biofilter. Inlet of the fluid (1.1), inlet chamber (1.2), lower flange components (1.3 and 1.5), lower perforated graphite plate (1.4), titanium screw and titanium contact cylinder (1.6), borosilicate glass cylinder (1.7), steel rods as counter electrodes (1.8), upper perforated graphite plate (1.9), feed spacer (membrane technology) (1.10), insulating plate (1.11), perforated hollow cylinder for isolation (1.12), titanium screw (connection) or plastic screw (isolation) (1.13), titanium rod (1.14), upper flange (1.15), steel plate for counter electrode attachment (1.16) with connection to the potentiostat (1.17), plastic ring to separate steel cover and steel plate (1.18), steel cover (19), lip seal ring (1.20) and top outlet (1.21). b: Photograph of the reactor with mounting. Gas trap with inlet (2.1), circulation outlet (2.2), siphon outlet (2.3), gas outlet (2.4), liquid sampling spot (2.5), and electrical heating pad (2.6).
c: Photograph of the packed bed of conductive spheres (3.1), upper perforated graphite plate (1.9).
d: Flow scheme of reactor and periphery. Reference electrode (4.1), pH electrode (4.2), potentiostat (4.3), sterile filter (4.4), gas flow meter (4.5), gas bag with nitrogen for volume compensation (4.6), peristaltic feed pump (4.7), peristaltic fluidisation pump (4.8), gear pump for circulation (4.9), feed bottle (4.10), and product collection bottle (4.11). Colour schemes show the possible operating modes. red: continuous mode, green: batch mode with recirculation, red plus green: continuous mode plus recirculation, blue: fluidisation mode.

of V4 steel. The steel cover is isolated from the steel plate (1.16) by a plastic ring (1.18). An insulating plate (1.11) separates the graphite plate (1.9) and the titanium rod. O-rings were installed as seals between components in contact with the environment. Because the packed bed length is too short for application of Delgado's approach for calculating axial dispersion in packed beds, the longitudinal Peclet number was estimated to be 0.53 based on results of the work of Hennico et al. [28].

The reactor is autoclavable, which makes white biotechnology applications accessible. The design decisions to improve or enable the packed bed reactor concept for easier scalability are the following: The distance between cathode and anode is independent from the packed bed height, which makes longer beds more accessible. Applying pressure on the packed bed enables better polarisation of the granules by lowering contact resistance between the granules.

2.2. Reactor periphery

A gas trap is installed close to the outlet of the reactor chamber with a liquid inlet (Fig. 1b, No. 2.1), two liquid outlets, one for recirculation (2.2) and the other designed as a siphon (2.3), which leads to a product collecting tank (4.11), a gas outlet (2.4), connected to a gas meter for volumetric flow measurement (Fig. 1d, No. 4.5; MilliGascounter MGC-1 V3. 4 PMMA, (RITTER Apparatebau GmbH & Co. KG, Bochum, Germany), and a liquid sampling point (2.5). Temperature control was carried out with a heating pad (2.6, HEWID Heizelemente GmbH, Berlin, Germany). For pH control, a pH electrode (Memosens CPS11E, Endress + Hauser, Reinach BL, Schweiz) (Fig. 1d, No. 4.1) and transmitter (Liquiline CM14, Endress + Hauser) were used. Voltage control was realised using an Ag/AgCl reference electrode (Xylem, SE23I, Xylem Analytics Germany Sales, Weilheim, Germany) (4.2) and a potentiostat (Interface 5000P, Gamry Instruments Inc., Warminster, USA) (4.3). Gas bags (4.6; RITTER Apparatebau GmbH & Co. KG, Bochum, Germany) with upstream sterile air filters (4.4) were used for pressure equalisation. A peristaltic pump (4.7; IPC, Ismatec, Cole-Parmer, Wertheim, Germany) (4.7) was used to feed the reactor with fresh medium from the feed reservoir (4.10), while a magnetic gear pump (4.9; magnetic gear pump PAT Niemzik, Haan, Germany) was used to recirculate the liquid phase. The valves and pumps are arranged in such a way that three different operating modes can be realised, as demonstrated in Fig. 1d: 1. continuous mode without recirculation, in which the substrate passes through the packed bed exactly once (red route), 2. batch mode with recirculation (green route), and 3. combination of both (red and green route combined). For the latter, the overflow velocity is decoupled from hydraulic retention time. However, in this work, results are obtained from operation mode 2 (green route) only. A peristaltic pump (M6–12 L Peristaltic Pump, Drifton, Hvidovre, Denmark) with high volumetric flow rates (4.8) is provided to fluidise the bulk material, if necessary (blue route). Therefore, the upper graphite plate has to be lifted to provide space for the expanding bed. Fluidisation aims to abrade biofilm from the spheres, as an excessively growing biofilm will lead to clogging of the biofilter and cause inhomogeneous flow of the liquid phase through the pore space. Pipes belonging to the blue and red routes between the final valve in front of the reactor inlet and the first valve behind the reactor outlet as well as the siphon were realised with an outer diameter of 12 mm (inner diameter: 10 mm), the rest of the periphery was realised with a diameter of 8 mm (inner diameter 6 mm) (1 d). The entire reactor can be drained via a three-way valve port (4.12).

2.3. Cultivation medium

All chemicals were purchased from the companies Carl Roth (Karlsruhe, Germany), Sigma-Aldrich (Germany), VWR International (Belgium) and Merck (Germany). The medium recipe was based on the M4 recipe of the Caroline Ajo-Franklin Research Group [29] and serves as a minimal medium for *S. oneidensis* (see supplementary information). The following changes were made: In this study, no lactate solution, but a 90 % (w/w) lactic acid solution was used as carbon source, which forms di-lactides at these high concentrations. To convert this di-lactide back into lactic acid and prevent di-lactide occurrence in the medium, the solution was diluted to 140 mmol L^{-1} and autoclaved. After that it was diluted to the final concentration of 70 mmol L^{-1} of lactate according to the recipe. The combined mass of yeast extract and tryptone was replaced by the same amount of casein hydrolysate. The Good-Buffer MOPS was used for pH-stabilisation at a concentration of 22.88 g L^{-1}, which equals 70 mmol L^{-1} deprotonated MOPS at a pH of 7.4. After autoclaving, sterile filtered kanamycin was added to a final concentration of 50 μg mL^{-1}. Sterile filtered arabinose was supplemented to a concentration of 100 μmol L^{-1} to induce pBAD-promoter expression. Sodium hydrogen carbonate was not used, as the completed medium was stripped with nitrogen gas before the filling process.

2.4. Inoculum preparation

A genetically modified strain of *S. oneidensis* with overexpression of the *speC*-gene and deletion of λ prophage genes was used as described by Juergensen [11]. LB medium mixed with kanamycin (50 mg L^{-1}) was used to aerobically cultivate the bacteria on agar plates at 30 °C for 30 h. After transfer of a single colony into an Erlenmeyer flask filled to 20 % with LB-medium containing kanamycin (50 mg L^{-1}), growth in an incubator (30 °C, 40 rpm) continued for another 20 h up to an OD_{600} of 1. A single washing step was conducted by separating the bacteria from the LB medium using a centrifuge (3600 rcf, 10 min) and resuspending the pellet in washing medium. The latter equals the cultivation medium described in 2.2, but without organic substrate. Inoculation of the autoclaved reactor was done with 50 mL of inoculum of an approximate OD_{600} of ~30. This corresponds to approximately 0.78 g dry biomass, equivalent to 0.39 g cellular protein, estimated from optical density–biomass correlations reported for S. oneidensis cultivated in shake flasks [30]. Exact biomass amount was not determined.

2.5. Liquid and gas sampling

Liquid and gas samples were taken every one to two days. Liquid sampling was carried out with a sterile syringe and cannula through an opening fitted with a septum at the gas trap, which is located directly above the inlet (Fig. 1b, No. 2.5). OD_{600}, organic acids (Lactate, acetate, propionate and butyrate), TOC and DOC were measured. For the Total Organic Carbon (TOC), the unfiltered liquid sample was measured using a Shimadzu TOC-LCPH analyser (Shimadzu Deutschland GMBH, Duisburg, Germany), while the dissolved organic carbon (DOC; Shimadzu TOC-LCPH analyser) and the acids were determined after filtration of the sample (Polytetrafluorethylen, pore size 0.45 μm). A Metrohm 881 Compact Pro Ion Exchange Chromatograph (Metrohm Deutschland GmbH & Co. KG, Filderstadt, Germany) with a Metrosep Organic Acids 250/7.8 column was used to determine the acid concentrations. Acid monitoring covered lactate and acetate as main expected constituents as well as formate, propionate, butyrate, isobutyrate, valerate, and isovalerate as possible indicators of contamination.

For gas sampling, a gas bag with a capacity of 100 mL was connected to the gas trap behind the sterile filter. The composition of the gas was determined using gas chromatography. A 490 Micro GC (Agilent Technologies, Waldbronn, Germany) was used with the carrier gases argon and helium and the two stationary phases in "PoraPLOT U" and "CP-Molsieve 5 Å" Plot J&W GC columns (Agilent Technologies, Germany). Standard pressure and a temperature of 60 °C were applied. The volumetric flow of the exiting gas was recorded by a MilliGascounter® (RITTER Apparatebau GmbH & Co. KG, Bochum, Germany). Gas monitoring included hydrogen, carbon dioxide, oxygen, nitrogen, and methane.

2.6. Potentiostat applications

Voltage control and electrical current measurement were carried out using an Interface 5000P (Gamry Instruments Inc., Warminster, USA) with a chronoamperometric setting. The packed bed served as the working electrode and anode and was poised at 0 mV relative to the SHE in the beginning. This state persisted until the negative current, caused by the release of electrons from the packed bed for the reduction of residual oxygen in the liquid phase, stopped. After inoculation, the anode potential was adjusted to 300 mV vs SHE for the rest of the experiment. The quantity of electrons transferred to the anodic packed bed was deduced by integrating the measured current over time.

2.7. Procedure of the experiments

This paper presents the performance of the reactor prototype in two experiments conducted as repeated fed-batch processes. After sterilisation of the reactor units using an autoclave (Systec GmbH, VE-95, Linden, Germany), the units were assembled in a sterile bench and/or under a flame. A volume of 2.9 L of the sterile cultivation medium was transferred into the reactor and abiotically exposed to an anodic packed bed potential of 0 mV vs SHE for several hours. The inoculum was added to the system to reach a target OD_{600} of approximately 0.6. The potential of the anode was then increased to 300 mV vs SHE to facilitate the transfer of electrons obtained through oxidation reactions catalysed by the bacteria, while the cultivation medium was recirculated at a relative velocity between liquid and spheres of the packed bed of 0.05 up to 0.3 mm s^{-1}. This filter velocity or interstitial velocity is calculated from the volumetric flow rate $\dot{V}$ divided by the reactor cross-section of the packed bed A that was reduced to the void fraction ε as in Eq. (1).

$$u_F = \frac{\dot{V}}{A \cdot \varepsilon} \tag{1}$$

Changes in the filter velocity were carried out to check possible mass transport limitations between the bulk phase and the biofilm. The experiments were carried out as repeated fed batch operations: After the current density finally regressed from an observed maximum current, a part of the medium was exchanged or substrate (only carbon source) was spiked. The application of these different feeding methods was done to evaluate their impact on current production. Exchange of the bulk phase results in the dilution of the product, the renewal of nutrients as well as the removal of planktonic biomass, whereas spiking mainly leads to further accumulation of the product. This was immediately followed by a 30-minute mixing process via the circulation pump at a relative velocity between liquid and packed bed of 1 mm s^{-1}. The new batch was considered to begin when the previously set overflow speed was restored.

At the beginning of all biotic experiments, current density increased rapidly within a few minutes after the inoculation step. Abiotic control experiments (without inoculation) showed (relatively) unchanging current density in the range of −0.28 to 0.02 mA m^{-2} for several hours. Monitoring of *S. oneidensis'* cell attachment was done by measuring the optical density of the liquid samples. Table 1 lists the operation parameters of the batches.

Table 1
Operation parameters for each of the batches.

Batch	time range h	Filter velocity mm s^{-1}	initial pH	pH range	substrate addition
Experiment 1 Batch 1 $E1_1$	0–160	0.05	7.4	7.4 to 6.8	initial
Experiment 1 Batch 2 $E1_2$	160–280	0.22/0.05	7.2	7.4 to 7	exchange
Experiment 1 Batch 3 $E1_3$	280–373	0.06	7.4	7.4 to 7.1	exchange
Experiment 1 Batch 4 $E1_4$	373–466.8	0.06/0.12	7.2	7.3 to 7	exchange
Experiment 1 all batches $E1_{total}$	0–466.8	-			-
Experiment 2 Batch 1 $E2_1$	0–111.65	0.15	7.4	7.4 to 6.9	initial
Experiment 2 Batch 2 $E2_2$	111.7–163	0.30	7.15	7.2 to 7.0	spike
Experiment 2 Batch 3 $E2_3$	163–167	0.30	7.0	-	spike
Experiment 2 Batch 4 $E2_4$	169–301.2	0.30	7.4	7.4 to 6.9	exchange
Experiment 2 all batches $E2_{total}$	0–301.2	-			

Anode:

$$C_3H_6O_3 + H_2O \rightarrow C_2H_4O_2 + CO_2 + 4\ H^+ + 4\ e^- \tag{2}$$

Cathode:

$$4\ H^+ + 4\ e^- \rightarrow 2\ H_2 \tag{3}$$

Lactate is oxidised to acetate at the anode with the release of carbon dioxide, protons and electrons as shown in Eq. (2). The electrons are transferred from the anode surface to the cathode, where the protons, which reached the cathode via transport through the liquid phase, get reduced to hydrogen as shown in Eq. (3). The amount of electrons from the turnover, measured as current, is divided by the anode surface and is hence presented in the further text as current density *J*. Hydrogen and carbon dioxide were the sole components in the gas samples, apart from occasional nitrogen occurrences after medium exchange, which were attributable to prior anaerobisation. For balancing carbonate species, molar flow of CO_2 was subtracted from the amount of CO_2 which was stoichiometrically expected from the measured lactate conversion to acetate. The remaining amount was considered to be dissolved CO_2 in the liquid phase. The CO_2 content in the exhaust gas and concentration of this dissolved CO_2 matched the expectation according to Henry's law. Direct measurement of carbonate species concentration in the liquid phase was not performed.

The pH value in experiment E1 ranged between 7.4 and 6.8, decreasing steadily in each fed-batch after each increase caused by the exchange of media. This can be explained by the production and dissolution of CO_2 in combination with an insufficient buffer capacity of the solution. An excessive pH reduction was compensated by adding NaOH with a concentration of 5 mmol L^{-1} (20 mL each) at hours 113 and 260.

The planktonic cell density, measured as OD_{600} decreased continuously until the first liquid exchanges in both experiments, which might be ascribed to cell attachment, simple sedimentation and/or lysis, which are not compensated by planktonic cell growth (absolute values of OD_{600} are shown in Supplementary Information, Fig. 1). Since the onset of current production started right after inoculation, at least a part of this loss will be due to cell attachment to the anodic packed bed. The general suitability of the material for bacterial attachment was proven in precursor experiments with flat anodes of the same material and surface treatment, cultivated in vertically arranged flow cells with the same *S. oneidensis* strain. Surface monitoring with confocal laser scanning microscopy (CLSM), after 1 week cultivation time and a maximum

3. Results and discussion

3.1. Reactor functionality validation

The functionality of the reactor was tested in the anodic cultivation of *S. oneidensis,* performing anaerobic oxidation of lactate to acetate during the course of two experiments, which were run as fed-batches. In Experiment 1, medium was replaced with fresh medium, while in Experiment 2, medium was spiked with lactic acid. During this conversion, the following net reactions take place at the electrodes:

current density of 60 mA m^{-2} reached, indeed revealed cell attachment, but surface coverage was low and a maximum of only 1–2 layers of bacteria were detected (data not shown). However, attachment was not evaluated by image analysis in this study, as picking particles from evenly distributed regions in the packed bed is prone to oxygen access and aerobic growth during the collection time. Quejigo et al. built a reactor especially for this purpose by implementing special sampling ports [17].

As described in chapter 2.7, in the course of experiment E1, old medium was replaced with fresh medium three times over the course of 20 days. Results are shown in Fig. 2a, where the measured parameters current density *J*, quantity *V* and quality of the gas produced, and the concentrations *c* of lactate and acetate are plotted against time.

As can be seen, lactate concentration was 70 mmol L^{-1} at the

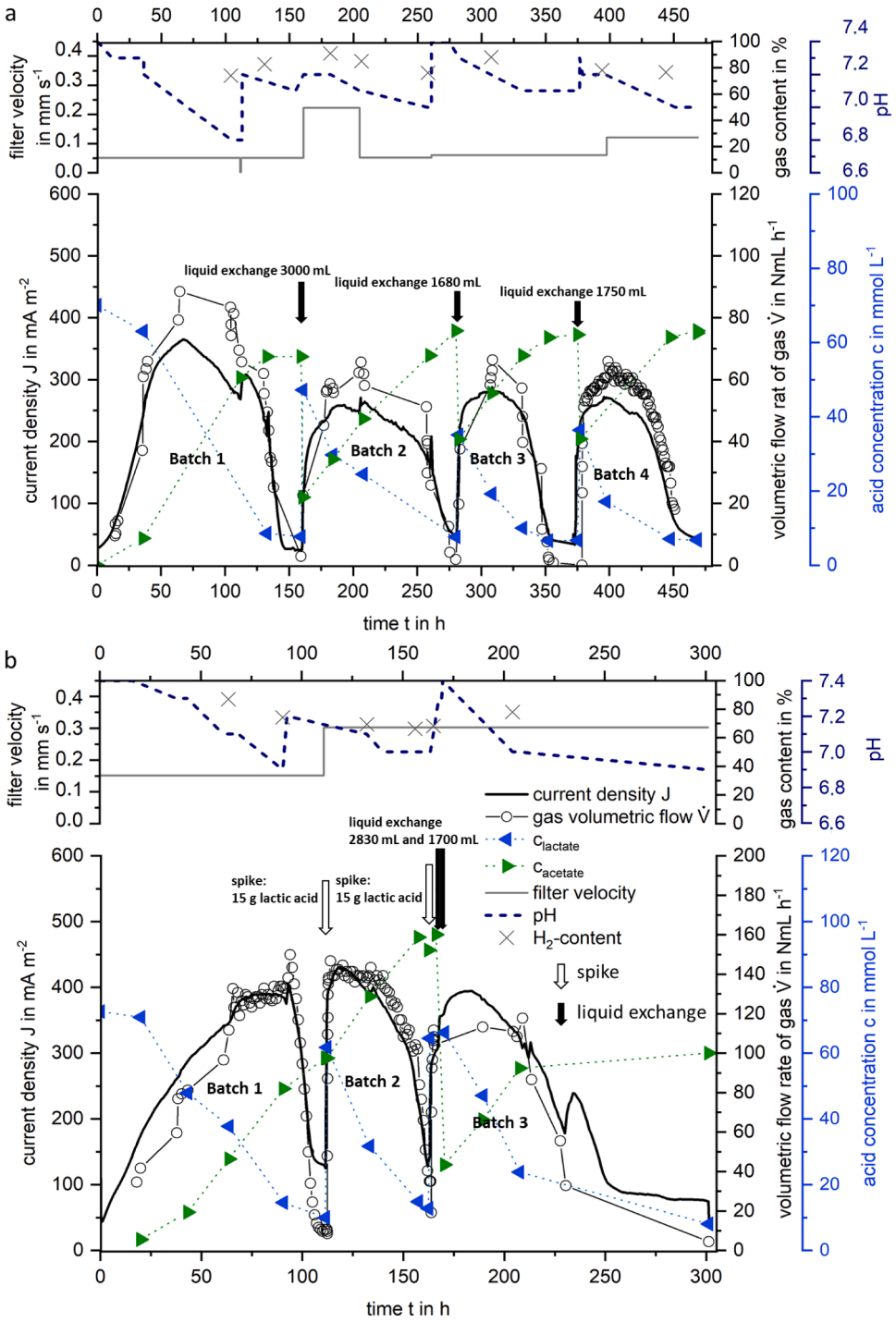

Fig. 2. Cultivation courses of experiments E1 (a) and E2 (b) performed with an anode potential of 300 mV versus SHE and at a temperature of 30 °C. Plotted values comprise the achieved current densities J, the volumetric flow rates of the exiting gases V, the percentages of hydrogen in the exiting gases (the remaining portion is carbon dioxide), the concentrations c of lactate and acetate, the filter velocities through the bulk anode material, and the pH values. The legend for both figures is shown in Fig. (b). Black arrows denote the times at which medium exchange took place (in (a): 159.3 h: 3000 mL, 280 h: 1680 mL, 375.4 h: 1750 mL; in (b): 167.0 h: 2830 mL,169.3 h: 1700 mL), white arrows denote the times at which spikings with lactic acid were performed (in (b): 111.7 h and 163.0 h; here, 15 g lactic acid equals 51.7 mmol L^{-1}).

beginning of experiment E1 and was reduced to 8.6 mmol L^{-1} over the course of batch 1 until hour 133In parallel, the acetate concentration rose from 0 mmol L^{-1} to 56.2 mmol L^{-1} at hour 133, confirming the incomplete turnover of lactate. This phenomenon of incomplete lactate turnover was observed throughout both experiments and might be attributed to an inhibitory effect of the high acetate concentration on lactate turnover, which will be discussed in more detail later. As shown in Fig. 2a, in the beginning of experiment E1 the steep increase of current density started at the same time, when the major part of lactate degradation took off respectively the acetate concentration rose, thus current development and acids changes correlated according to Eq. (2). Since sampling of the liquid phase was not as frequent as the electrical current measurement, the current density is the decisive indicator for the metabolic situation of the microorganisms as it is. It can be stated that after inoculation at time 0, a lag phase, where no turnover happens, did not occur, yet a little delay in the curve ascent can be seen for the first hours. The current density rose to the local maximum of 365 mA m^{-2} until hour 69 (peak 1), declined afterwards and then started to fall sharply from 301 mA m^{-2} at hour 120 to a local minimum of 26 mA m^{-2} at hour 147, where it remained relatively constant during the following 13 h of cultivation.

At the point of stagnation (hour 159), a part of the medium was replaced in order to replenish the substrate supply. The used medium was exchanged by turning off the recirculation pump and continuously adding fresh medium. Thus, the reactor liquid was exiting the reactor through the siphon. The volumetric flow rate of the added fresh medium corresponded to roughly four times the previous flow rate of the recirculation pump, and filter velocity was kept at this value of 0.22 mm s^{-1} for almost two days. As denoted in Fig. 2, the exchanged volume was 3 litres, added at hour 161, which is theoretically sufficient to completely replace the entire liquid phase of the reactor of 2.9 litres. This should result in a medium exchange of 90 percent (using Danckwerts calculation, details in supplementary information). However, due to dead zones in the entrance of the reactor the replacement of old medium was incomplete, so the lactate and acetate concentrations in the reactor after medium exchange did not reach the concentrations of the expected replacement of 63 mmol L^{-1} and 6 mmol L^{-1}, respectively. Instead, the lactate concentration was increased (from 7) to 47.2 mmol L^{-1}, whereas the acetate concentration was decreased (from 56.2) to 18.3 mmol L^{-1}, which corresponds to an exchange rate of 66 % for the liquid phase (for equation see supplemented information). With the start of the second batch (hour 161), the filter velocity was changed to 0.22 mm s^{-1} and back to 0.05 mm s^{-1} 43 h later. As no lasting changes in current density were observed, it is assumed that mass transfer limitations between bulk phase and biofilm can be considered negligible.

Medium exchange resulted in a rapid increase in current density to 213 mA m^{-2} within 10 h and a local maximum of approx. 261 mA m^{-2} 34 h after exchange. Compared to the first local maximum (peak 1), the second one (peak 2) is smaller, due to a lower substrate starting concentration and higher product concentrations throughout the second batch. High concentrations of acetate result in an inhibitory effect, which is explained in detail in chapter 3.2 [31]. At the end of batch 2 at hour 280, lactate concentration was 7.6 mmol L^{-1} and, thus, was close to the final concentration of batch 1 (7 mmol L^{-1}). Acetate concentration reached 63.2 mmol L^{-1}, and current density was at a minimum of 41 mA m^{-2}. For batches three and four, 45 % of the old medium was exchanged with new medium. Like before, medium exchange led to an analogous behaviour of lactate degradation and acetate production with correlating current densities.

Experiment E2 (Fig. 2b) differs from experiment E1 in that the liquid medium between batch 1 and 2, as well as 2 and 3, was not exchanged with fresh medium after substrate degradation but instead was spiked with pre-treated lactic acid (initially 90 %-ww). The pH value ranged between 7.4 and 6.9. Results of this repeated fed-batch experiment are shown in Fig. 2b, where the current density J, quantity V and quality of the product gas flow, the concentrations c of lactic and acetic acid, the filter velocity, the pH value and the hydrogen content in the gas phase are plotted against time.

As in experiment E1, the initial lactate concentration was 70 mmol L^{-1}, which was degraded to 10 mmol L^{-1} until hour 112 while the acetate concentration increased from 0 mmol L^{-1} to 58.5 mmol L^{-1}. Current production correlated with the lactate degradation and acetate production, respectively. Again, a lag phase could not be seen, and current density peaked at 392 mA m^{-2}, followed by a decline to 129 mA m^{-2} at hour 111. At this point, as 10 mmol L^{-1} lactate residual concentration was considered nearly depleted, 15 g of concentrated lactic acid was diluted to a volume of 22 mL liquid and set to pH 7.4 before being added via sterile filtration; thus, the initial lactate concentration of batch 2 was 61.7 mmol L^{-1}. As the liquid phase was only spiked, the acetate concentration was not reduced before the start of batch 2. However, within batch 2, lactate was depleted to 12.8 mmol L^{-1} at hour 162, while acetate and current were produced. Another spike with lactic acid was performed at hour 163 with the same concentration increase, Δc of 51.7 mmol L^{-1}; however, this did not have the same effect on the current density in batch 3 as the first spike in batch 2, but came to a halt (peak not visible in Fig. 2 due to temporal resolution) halfway to the expected peak. As it was suspected that the high concentration of acetate might inhibit the metabolism of *S. oneidensis*, part of the liquid phase was then replaced with fresh medium at hours 167 and 169.3, respectively, which led to an acetate concentration drop (96.0 mmol L^{-1} to 32.6 mmol L^{-1}) while the concentration of lactate stayed nearly the same (64.5 mmol L^{-1} to 57.1 mmol L^{-1}). As a result of this exchange, current density began to rise again (Fig. 3a and b: arrows to red and blue striped squares) and peaked at 394 mA m^{-2} at hour 182. Comparing these two peaks, both, state of the bacteria on the packed bed (peaks are only a few hours apart) and prevailing lactate concentrations are similar, while acetate concentrations differ by a factor of 3. It is thus concluded, that inhibition by acetate was responsible for the hampered increase of current density before medium exchange. At hour 207, the batch ends in terms of evaluable data, since interventions carried out on the reactor beyond this time point make further calculations very complex (and will not be discussed in detail here).

3.2. Inhibitory effect of acetate

The inhibitory effect of higher concentrations of acetate on *S. oneidensis* is described by Tang et al., where it is reported that concentrations of 30 mmol L^{-1} already showed a significant effect on the performance [31]. It is visualised in Fig. 3: For each of the single repeated batches of experiments E1 and E2, local maxima (peaks) and subsequent minima of current density exist. No such minimum exists for batch 3 of E2, as the lack of the anticipated high current density led to the decision of an immediate replacement of the medium which resulted in a subsequent maximum (see Fig. 3a). In Fig. 3b, these values are plotted against the concentrations of lactate that prevailed at these time spots (black squares) (for data point information see supplementary information).

Lactate concentrations never fell below 6.5 mmol L^{-1}. To be able to mathematically describe this offset in Fig. 3b, we applied an exponent to the concentration, similar to the Hill equation (Eq. (4)), which originates from protein ligand complex building phenomena. It was chosen over other kinetic approaches, like e.g. an adapted Michaelis-Menten approach, solely for mathematically reasons. It defines the relationship between reaction rate v and substrate (originally ligand) concentration c, with a constant maximum reaction rate v_{max}, an exponent n and a half saturation constant K_A.

$$v = \frac{v_{max} \cdot c^n}{{K_A}^n + c^n} \tag{4}$$

Applied to the experiment, the parameters would translate to current density J, maximum current density J_{max}, and lactate concentration $c_{lactate}$, accordingly (Eq. (5)). The half-saturation constant K_A denotes the

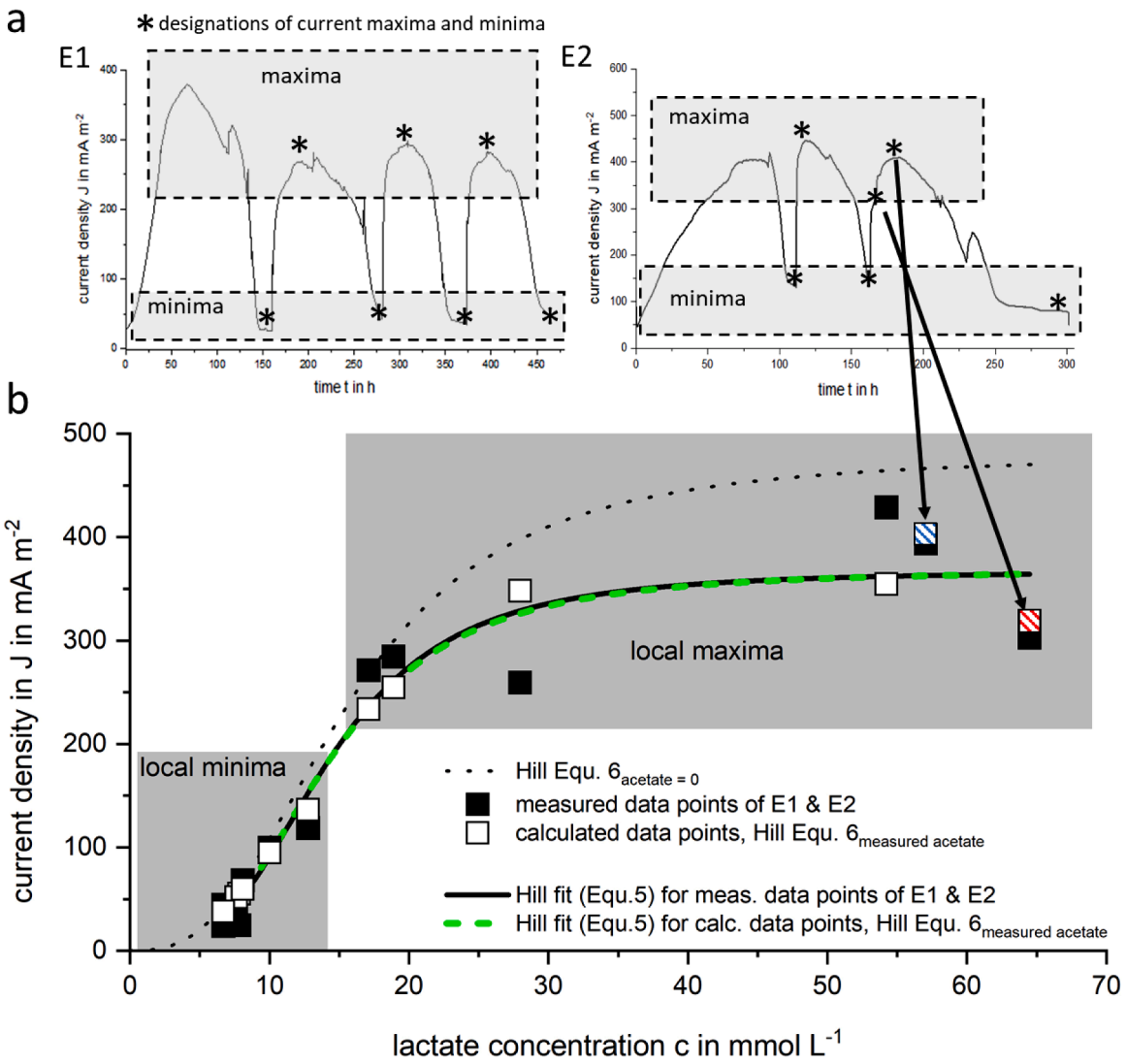

Fig. 3. a: Designations of local current maxima and minima (asterisks) of experiments E1 and E2 used in (b). b: Local maxima and subsequent minima of current densities of experiments E1 and E2 plotted against the associated lactate concentration (black squares). Local minima of the current, which were found shortly before changing medium or adding lactate, are displayed on the left side, whereas the maximum current densities (peaks) are displayed on the right (shadowed areas). The Hill fit for E1 and E2 (black line) is calculated based on the actual data points (black squares) of E1 and E2, omitting only the maxima of the first peaks of E1 and E2 as shown in (a). The dotted black line shows a plotted Hill equation (according to Eq. (6)) for a hypothetical acetate concentration of zero (thus, assuming no inhibition). The white squares represent the calculated local maxima and minima derived from this Hill plot (Eq. (6)) using the actual prevailing acetate concentrations, and thus considering product inhibition. Finally, the dashed green line shows the Hill fit based on the calculated maxima and minima (white squares) which were calculated using Eq. (6). The red- and blue-striped squares (belonging to the "calculated data points, Hill Eq. (6)" and connected with the corresponding peaks in Fig. 3a via black arrows) represent the current densities before (red-striped square) and after medium exchange (blue-striped square), where lactate levels remain similar, whereas acetate concentration was strongly reduced.

concentration $c_{lactate}$ at which the current density J reaches half of its maximum value J_{max}. The current densities shown at specific time points also include those resulting from hydrogen shuttling (which is explained in chapter 3.3). The impact of the latter is unknown, as it could only be observed as a sum effect over the length of the experiments.

$$J = \frac{J_{max} \cdot {c_{lactate}}^n}{{K_A}^n + {c_{lactate}}^n} \tag{5}$$

As discussed before, the acetate concentration has an inhibitory effect on lactate turnover and thus, current density. Therefore, the Hill approach of Eq. (5) was extended by two inhibition terms in Eq. (6). For the observed mitigation of turnover, either competitive or uncompetitive inhibition by acetate seems plausible. Tang et al. state that, among other things, the permeation of acetate through the membrane could cause a change in the intracellular pH value of 7.5 and hence, uncompetitively inhibit the formation of enzyme-substrate complexes. Additionally, they discuss the possibility that a conversion of acetate to acetyl-CoA might also directly compete for CoA groups with lactate by occupying them, hence limiting the lactate conversion rate [31]. Eq. (6) takes both options into account by considering competitive and uncompetitive inhibition.

$$J = \frac{J_{max} \cdot {c_{lactate}}^n}{{K_A}^n \left(1 + \frac{c_{acetate}}{K_i}\right) + {c_{lactate}}^n \left(1 + \frac{c_{acetate}}{K_{ii}}\right)} \tag{6}$$

Using this equation and the actual lactate and acetate concentrations prevailing at the corresponding local maxima and minima defined in Fig. 3a, the best possible approximation for the actually measured current densities (black squares) was sought. The parameters J_{max}, K_A, and the exponent n were set to 480 mA m^{-2}, 15.7 mmol L^{-1}, and 2.735, respectively. The value of K_A is close to the Michaelis constant of 14.5

mmol L^{-1}, as found by Renslow et al. for *S. oneidensis* and its anaerobic lactate to acetate metabolism using fumarate as terminal electron acceptor [32]. The competitive inhibition dissociation constant K_i was set to 600 mmol L^{-1}, whereas the uncompetitive inhibition dissociation constant K_{ii} was set to 200 mmol L^{-1}, thus, assuming a higher impact of uncompetitive inhibition. The resulting values of this calculation are depicted as white squares in Fig. 3b To complete the picture, an additional Hill curve is depicted as dotted black line. It is based on the exact same Eq. (6) and parameters, except that the acetate concentration is assumed to be 0 mmol L^{-1}, thus showing the hypothetical current density as it would appear without inhibition. Finally, the applicability of Eq. (6) is confirmed by the congruence of the Hill fits of the measured data points (black squares; fit: black line) and the calculated data points (white squares; fit: dashed green line) depicted in Fig. 3b They do not include the data of the initial batches (peaks "1″ of E1 and E2), as those differed from the subsequent batches due to incomplete establishment of the microbial culture. Both fits are based on Eq. (5) which does not mathematically consider inhibition. Nevertheless, this approach is valid since the inhibition is inherent in both data sets: the measured data points are influenced by the actual product inhibition caused by the presence of acetate during the experiments; the calculated data points result from Eq. (6) that includes both inhibition terms. The empirical character of Eq. (6) entails that further limiting factors in the reactor operation, like, e.g., substrate limitation, proton transport limitations to the cathode and/or local pH drops, are included but not defined.

3.3. Stoichiometric balance

An essential aspect in the operation of bioelectrochemical systems is a comprehensible electron balance. The time-integrated quantities of produced electrons (based on measured current densities) for each batch of experiments E1 and E2 are listed in Table 2. Furthermore, the corresponding electron quantities expected to be measured by the potentiostat, based on the measured lactate degradation and based on the production of acetate derived from Eq. (2) and (3), respectively, are given. Additionally, the electrons that went into measured hydrogen production, as well as the maximum degradation rates of lactate and maximum production rates of acetate of each batch, are given.

The produced acetate during batch 1 was 90 % of the amount of degraded lactate, while in the follow-up batches, acetate production matched 113 %, 99 % and 97 % of the amount of degraded lactate. This additional acetate synthesis might be explained by degradation of lysed cells and/or measurement inaccuracies. For all batches, the electrons transferred to the anode were roughly double of what can be explained by acetate production as defined in Eq. (2). As *S. oneidensis* itself is not able to metabolise acetate anaerobically, acetate degradation cannot be the source of these electrons. This is a strong indicator for the occurrence of so-called hydrogen shuttling or hydrogen-cycling as explained in detail in this chapter [33].

As can be deduced from the table, the amount of produced electrons recorded by the potentiostat is significantly higher than the amount of electrons that would be expected based on the measured degradation or production of the carbon compounds. The Coulombic efficiency (CE) (see supplementary information), which can be defined as the ratio between measured electrons (e^- current) and electrons that can theoretically be produced through substrate decomposition (e^- degraded lactate), amounts to 206 % for experiment E1 and 141 % for experiment E2. Usually, the maximum CE is limited by default to 100 %, that is, when all substrate is utilised in catabolic metabolism and no substrate is used as a carbon source for anabolic pathways. The obtained, very high CEs for both experiments can only be explained by *S. oneidensis'* ability to metabolise hydrogen [34]: This leads to a loop of electron uptake and release in the form of hydrogen shuttling as seen in Fig. 4, where a part of the already produced hydrogen at the cathode is oxidised by the bacteria, leading to electron transfer to the anode without any further lactate degradation involved. This is possible, because the potentiostat is providing free energy by maintaining the voltage to continue this shuttling.

Hirose et al. [33] also described this phenomenon when they oxidised lactate to acetate using a BES. The hydrogen shuttling by *S. oneidensis* can be prevented, though, by deleting its hydrogenases without compromising its ability to oxidise carbon sources [33].

However, since an electron resulting from substrate degradation can leave the reactor system as hydrogen via the gas trap only once, the measured hydrogen production is stoichiometrically still relatable to the formation of its metabolic co-product acetate and to the degradation of lactate, even if much more hydrogen was produced during the experiments than harvested. For the entire experiment 1, the total amount of measured hydrogen per batch was just 80 % of what would be expected from acetate production, associated proton release and conversion to hydrogen. The missing part of the hydrogen produced is considered to be lost through intermittent leakage at the sampling point (Fig. 1b, 2.5) in the gas trap releasing hydrogen after a certain unknown pressure threshold, noticed only after the first experiment was completed. After the leak was fixed, the ratio of expected and measured hydrogen increases to 94 % for experiment E2.

Contamination of experiments was considered unlikely for several reasons: The use of antibiotics suppresses the growth of alien bacteria. Methane, a common but unwanted by-product of biological hydrogen production, could not be detected in the gas samples. In general, only lactate, acetate, carbon dioxide and hydrogen were found in the samples, and the amounts are considered stoichiometrically balanced with reasonable deviations. Short-chain fatty acids other than the named ones were not detected. Finally, the imbalance of measured electrons and degraded lactate (CE over 100 %) can be explained by *S. oneidensis* capability of hydrogen shuttling.

Table 2
Electron balances of experiments E1 and E2, given as time-integrated values for each batch ($E1_1$ to $E1_4$; $E2_1$, $E2_2$ and $E2_4$) and as a sum for each experiment ($E1_{total}$ and $E2_{total}$). The time range of each batch and filter velocity are given. e^- current: the current recorded by the potentiostat during the respective time period, e^- degraded lactate and e^- produced acetate: the amount of current that should have been delivered to the anode based on the measured degradation of lactate (Eq. (2)) and the measured production of acetate, respectively (Eq. (3)), e^- harvested hydrogen: the amount of current required for the production of the measured harvested hydrogen. The maximum degradation rates of lactate and the production rates of acetate for each batch are also given. Batch 3 of E2 ($E2_3$) is excluded due to its incompletion.

Batch	time range h	e^- current mol	e^- degraded lactate mol	e^- produced acetate mol	e^- harvested hydrogen mol	maximum lactate degradation/ uptake mmol L^{-1} h^{-1}	maximum acetate production mmol L^{-1} h^{-1}
$E1_1$	0–160	1.43	0.72	0.65	0.60	−0.56	0.57
$E1_2$	160–280	0.97	0.46	0.52	0.40	−0.79	0.45
$E1_3$	280–373	0.69	0.33	0.33	0.26	−0.61	0.48
$E1_4$	373–466.8	0.71	0.34	0.33	0.26	−0.95	-
$E1_{total}$	0–466.8	3.81	1.85	1.91	1.52		
$E2_1$	0–111.65	1.17	0.70	0.68	0.66	−0.99	0.80
$E2_2$	111.7–163	0.71	0.57	0.38	0.38	−1.42	0.89
$E2_4$	169–207.5	0.6	0.49	0,41	0.34	−1.128	0.86
$E2_{total}$	0–207.5	2.48	1.76	1.47	1.38		

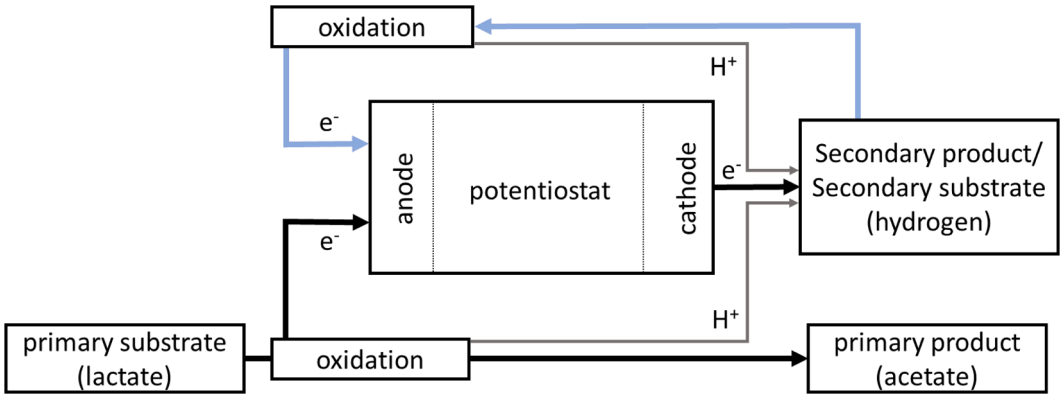

Fig. 4. By-pass process of "hydrogen shuttling" decoupled from the original primary degradation pathway. Hydrogen is used as a secondary substrate by the microorganisms It simultaneously is formed as a secondary product on the cathode, thus leading to the reading of a significant excess of electrons by the potentiostat, which cannot be explained by degradation of the primary substrate alone.

3.4. *Degradation rate of lactate and production rate of acetate*

The rate of maximum lactate absorption or degradation of each batch in Table 2 is significantly higher compared to the corresponding maximum acetate production, with the latter being only 20 to 40 % of the former. Also, the degradation rate of lactate is always higher at the beginning of the batches and decreases over time, while the production rate of acetate is relatively constant over the duration of the batches (data not shown). Because the overall stoichiometry of lactate and acetate is balanced, it is assumed that there is some delay from lactate uptake to acetate excretion, although, to our knowledge, no evidence of this phenomenon has been described in the literature yet.

No correlation was found between the maximum production rates of acetate and the chosen filter velocity, when each of the experiments is evaluated separately (Fig. 5a). Typically, a higher filter velocity leads to a better supply of the biofilm with nutrients or disposal of products due to the reduced diffusive boundary layer and its effect on internal substrate gradients [35]. However, formation of thick biofilms is unlikely for *S. oneidensis* grown under anoxic conditions [22] and it was also proven in preliminary experiments (data not shown) performed in a MEC-flow cell described by Hackbarth et al. [36] that the attachment of *S. oneidensis* cells to the conductive substratum led to individual

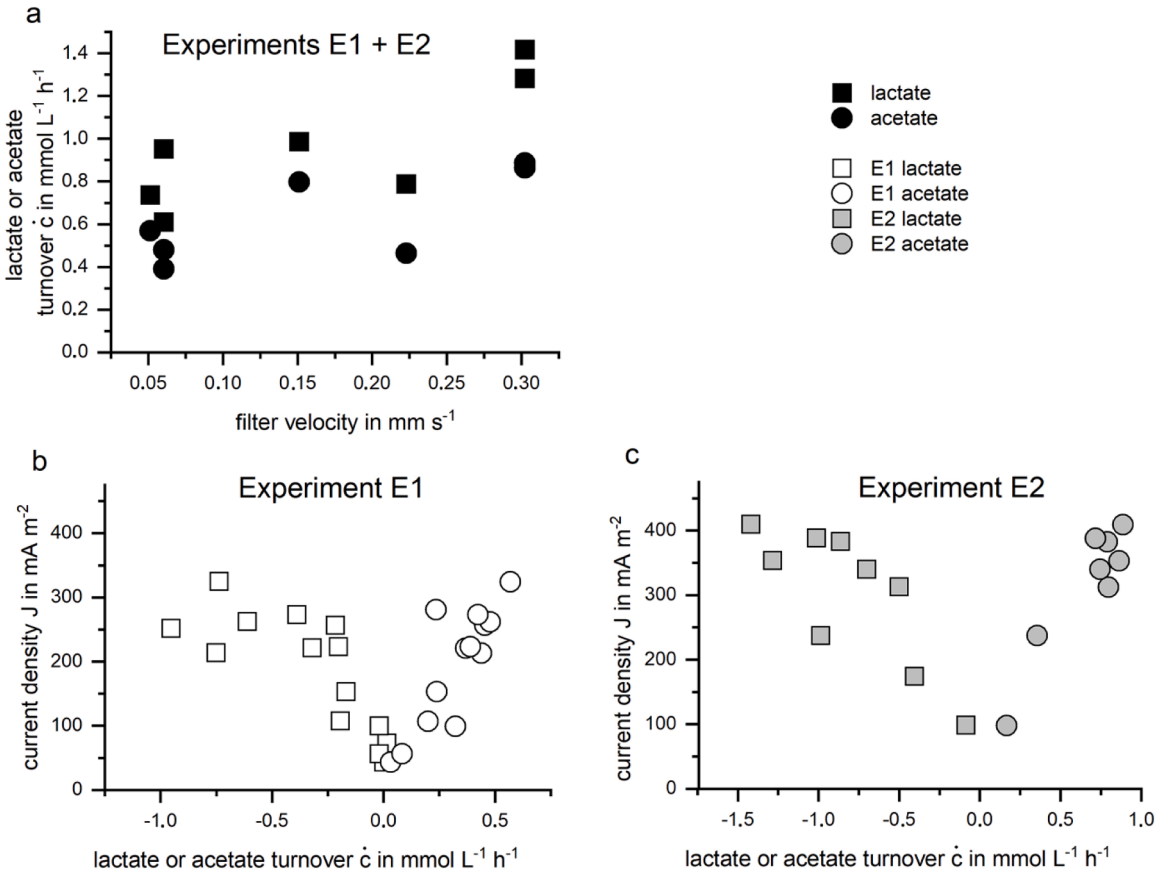

Fig. 5. a: Maximum acetate production rates as well as lactate uptake rates of each batch/repeated fed-batch of experiments E1 and E2 plotted against the calculated filter velocity at the time of the maximum production rate of the chosen batch. b and c: Average current density plotted against the lactate uptake rates, as well as against the acetate production rates of experiments E1 (b) and E2 (c).

distributed cells or very thin biofilms consisting of up to 2 cell layers, so substrate limitation of the biofilm was not expected and the chosen filter velocity considered to guarantee sufficient supply.

Fig. 5b and c (for calculation of data points, see supplementary information) show the correlation between the average current density and lactate uptake and acetate production for both experiments. As expected, the detection of acetate also increases linearly with higher current density as its production is inherently connected (see equation Eq. (2)). For experiment 1 (Fig. 5b), there seems to be a threshold value of approx. -0.4 mmol L^{-1} h^{-1} lactate turnover for which, when exceeded, the uptake rates of lactate are not reflected in higher acetate production rates. The same is true to a lesser extend for E2 (Fig. 5c), where the uptake rates >-1 mmol L^{-1} h^{-1} are not reflected by higher acetate production rates. This can be attributed to the delay of acetate output mentioned above.

The maximum acetate production rate reached 0.89 mmol L^{-1} h^{-1} or 3.6 g m^{-2} d^{-1}, while the maximum lactate uptake/degradation reached 1.42 mmol L^{-1} h^{-1} or 5.7 g m^2 d^{-1}, respectively.

3.5. Classification of the production rates in light of the current literature

In general, comparing BES is not a simple task: One initial challenge lies in comparing the active electrode area, which is one of the key factors determining the resulting current densities. For example, electrode brushes or felts have high effective surfaces, they are usually characterised only by the outer surface of the complex 3D-structure; thus, the calculated current densities are overestimated in comparison to the values obtained on solid electrode surfaces. Similarly, incomplete polarisation of packed bed anodes changes the assumed surface area, which is derived solely from a formal calculation. Second, the degree of oxidation of an organic substrate (to carbon dioxide), and, consequently, the release of stoichiometrically more electrons per mol of degraded organic substrate, inherently increases current density. E.g., literature found for comparison as listed in Table 3 focus mostly on the total oxidation of substrate to carbon dioxide providing double or even triple amounts of released electrons per substrate compared to the partial oxidation of lactate as it was performed in this study. Finally, differences in applied voltages worsen comparability, because they affect facilitation of turnover rates and may even open up new metabolic degradation pathways at different potentials [37]. Nonetheless, to assess the reactor performance, Table 3 lists other concepts of single-chamber reactors for comparison.

A single-chamber BES design approach of such a scale-up experiment for H_2 production is shown by the 2.5 L MEC-reactor of Rader & Logan [6]. Eight graphite fibre brushes as anodes (working electrode) and eight steel mesh units as cathodes were arranged as electrode pairs within one container. The reactor was fed with an acetate solution of 1 g L-1 and inoculated with an undefined mixed culture from an MFC also fed with acetate [6]. In another study, a similar but larger MEC of 1000 L volume was equipped with 144 electrode pairs of graphite fibre brushes/stainless steel meshes and inoculated with wastewater sludge [7]. Both reactors were used to continuously produce hydrogen from an organic carbon source, but over the course of experiments, in both studies, the product gases shifted from H_2/CO_2 mixtures to mainly methane. The cathodic target product, hydrogen, was largely converted by hydrogenotrophic methanogenic archaea before it could be harvested from the reactors. The scale-up of the fibre brush concept from 2.5 to 1000 litres, while using more or less similar substrate load, though applied by different researchers, led to a decrease of 90 % of the achieved current density, showing the challenges of scaling-up.

Another recent example of a scaled-up MEC is a 10-L upflow reactor with dimensions of 1 m length and a square cross-section edge length of 10 cm. The cultures for inoculation were derived from the digested sludge of a wastewater treatment plant and fed with a substrate mixture of 50 mmol L^{-1} acetate and 11.1 mmol L^{-1} glucose. The flat anodes were made of carbon cloth and braced in frames along the direction of flow. With an anode cloth surface of 1 m^2 and an applied voltage of 1000 mV relative to SHE, a surface-related current density of 34 A m^{-2} and a reactor volume-related current density of 970 mA L^{-1} were achieved [38]. Comparison to this study is difficult as the high voltage applied and higher operation temperature of 37 °C favour high current density.

The use of solid, planar electrodes was realised by Hackbarth et al. [9] who chose a rotating disc design with a working electrode surface area of 1 m^2 and a reactor volume of 10 L. It was originally designed for microbial electrosynthesis but was also operated as MEC to cultivate a mixed culture of *Shewanella oneidensis* and *Geobacter sulfurreducens* with the anode poised teat 0 mV vs. SHE. In a series of batch experiments of 9 days, with a starting substrate concentration of 20 mmol L^{-1} of each

Table 3
Overview of current densities achieved in scaled-up MEC for comparison with the biofilter of this study.

Reactor type	Anode material	Anode voltage in mV vs SHE	Reactor volume	WE surface in m^2	Current density	Medium	Product	Inoculum	Reference
Cube type	Graphite brushes	900	2.5 L	0.051	72 mA L^{-1}	16.6 mmol L^{-1} acetate, conti.	CO_2, H_2	MEC culture	[6]
Cube type	Graphite brushes	900	1000 L	15.2	7.4 mA L^{-1}	0.7–2 g L^{-1} VFA, conti.	H_2,CO_2	Digester sludge wastewater	[7]
Elongated up flow	Carbon cloth	1000	10 L	1	34,000 mA m^{-2} 970 mA L^{-1}	50 mmol L^{-1} acetate 11.1 mmol L^{-1} glucose, conti.	H_2,CO_2	wastewater digester sludge	[38]
Rotating disc	Graphite plates	0	10 L	1	1300 mA m^{-2} 130 mA L^{-1}	20 mmol L^{-1} acetate 20 mmol L^{-1} lactate, conti.	H_2,CO_2	*S. oneidensis* and *Geobacter sulfurreducens*	[9]
Rotating disc	Graphite plates	200	10 L	0.5	1800 mA m^{-2} 90 mA L^{-1}	20 mmol L^{-1} lactate, fed-batch	H_2,CO_2	*S. oneidensis* and *Geobacter sulfurreducens*	[10]
Rotating disc	Graphite plates	0	10 L	0.5	1200 mA m^{-2} 60 mA L^{-1}	20 mmol L^{-1} lactate, fed-batch, 160 μmol L^{-1} Riboflavin	Acetate, H_2, CO_2	*S. oneidensis*	[11]
Rotating disc	Graphite plates	300	100 L	10	240 mA m^{-2} 24 mA L^{-1}	25 mmol L^{-1} acetate 25 mmol L^{-1} lactate, batch	H_2,CO_2	*S. oneidensis* and *Geobacter sulfurreducens*	[12]
Granular packed bed	Gaphite granulates	400	2.7		134.3 mA L^{-1}	20 mmol L^{-1} acetate, fed batch	H_2,CO_2	*Geobacter sulfurreducens*	[17]
Granular packed bed	Carbon- polymer compound spheres	300	3.57 L	1.06	430 mA m^{-2} 128 mA L^{-1}	70 mmol L^{-1} lactate, repeated fed batch	acetate, H_2, CO_2	*S.oneidensis*	this study

lactate and acetate, a maximum surface-related current density of 1300 mA m^{-2} was measured, which equals a reactor volume-related current density of 130 mA L^{-1}, a result comparable to the current density achieved in this study.

A very similar experiment in the same reactor type but with half the anode surface (0.5 m^{-2}) was carried out as a repeated fed-batch experiment and showed a maximum current density of 1800 mA m^{-2} with the anode poised at 200 mV vs SHE. A stable current density of 1200 mA m^{-2} and 90 mA L^{-1}, respectively, could be maintained over 1.5 months with a maximum substrate supply of 20 mmol L^{-1} of lactate [10].

In this context, the work of Juergensen et al. has to be mentioned, who achieved an increase in performance in the same reactor configuration solely by optimising the medium with 160 μmol L^{-1} riboflavin. *S. oneidensis* was then able to generate current densities that would otherwise only be obtained in mixed cultures of *S. oneidensis* and *G. sulfurreducens*, indicating that riboflavin can compensate for the fact that *S. oneidensis* is unable to develop nanowires [11]. This might be a useful method to enhance feasibility of pure strain *S. oneidensis* for white biotechnology.

A scaled-up version is the 100 L RDBER investigated by Prakash et al., performing at 240 mA m^{-2} or 24 mA L^{-1}, showing that the scale-up of the rotating disc concept is promising, yet needs optimisation [12].

A current density of 134 mA L^{-1} was reached in the packed bed reactor with *Geobacter sulfurreducens* cultured in acetate medium by Quejigo et al. [17]. Compared to their results, compressing the packed bed as was done in this study is assumed to enhance polarisation based on the following observations: according to their displayed reactor configuration, the ratio of packed bed volume to reactor volume is nearly the same as it was in this study, but formal surface area in their set-up is higher due to usage of smaller granules. Also, *S. oneidensis* is a less suitable microorganism for anaerobic biofilm formation and only gains half of the electrons in its anaerobic metabolic pathway in lactate turnover than *G. sulfurreducens* does growing on acetate. This consequently reduces the current density of a BES. And finally, the voltage applied by Quejigo et al. [17] was higher than in this study. Still, similar current densities were achieved, indicating that the effective surface of the packed bed was higher in this study. This claim can also be supported by determining the anode surface via Fe^{2+} to Fe^{3+} conversion and chronoamperometry [39]. From this, an anode surface of 0.6 ± 0.12 m^2 was derived, which equals a portion of about 57 ± 11 % of anodic packed bed that is considered polarized (see supplementary material) in contrast to the 10 % reported by Quejigo et al. [17]. However, it has to be noted, that Quejigo et al. determined this portion by considering the granule surface which actually carried biofilm. Another reason for the current densities might be the reduced distances between anode and cathode, which should help to reduce proton concentration, and, thus, prevents unwanted pH shifts as well as reduces the impact of thermodynamic hindrance by accumulating product.

Despite the limited comparability of different reactor types, the current densities achieved in this study indicates that a BES with a polarised packed bed can be a useful reactor configuration for the scaled-up production of chemicals via electro-fermentation.

4. Conclusions

The functionality of the introduced biofilter as reactor design for electro-fermentation in white biotechnology was proven by the model conversion of lactate to acetate in terms of a proof of concept. The drawback of using electricity as driving force for the microbial reaction should be compensated by the production of a high-value chemical.

Maximum current density achieved was 430 mA m^{-2} at a voltage of 300 mV vs SHE at a lactate concentration of about 60 mmol L^{-1} and a maximum degradation rate of 1.42 mmol L^{-1} h^{-1}. With a reactor volume of 3.57 L and a surface of 1.06 m^{-2}, the maximum volumetric current density amounted to 128 mA L^{-1}. Higher productivities are expected for experiments with better biofilm formers, such as co-cultures of *S. oneidensis* and *G. sulfurreducens*, outside a proof-of-concept trial. The scale-up potential lies in the more pronounced polarisation of the packed bed by compressing the granules, rendering up-scaling by increasing packed bed volume more accessible. At a certain point, further scale-up and increased distance between connecting electrodes and the bed might lead to decreased bed polarisation, which might to be either counteracted by additional normal force on the packed bed or additional anode enhancements (e.g. bars) inserted sideways into the packed bed. Such adjustments, depending on size and form, are unlikely to interfere with the biofilm control option by fluidisation, a feature, which is, as in the case of cultivation of poor biofilm formers like *S. oneidensis*, not always needed

The flow through the reactor proved to be non-uniform due to dead zones as can be derived from the mixing of new and old medium after the refilling processes. It was addressed by adding perforated baffle plates in the inlet chamber (further information in supplementary information), but the experiments shown in this work were carried out without them. Other possible solutions would be funnel-shaped deflectors aligned in the radial flow direction in the inlet chamber, which would homogenise the flow at the inlet points of the filling body in the lower electrode disc.

CRediT authorship contribution statement

Maximilian Miehle: Writing – original draft, Methodology, Investigation, Data curation, Conceptualization. **Johannes Gescher:** Writing – review & editing, Conceptualization. **Harald Horn:** Writing – review & editing, Supervision, Funding acquisition, Conceptualization. **Andrea Hille-Reichel:** Writing – review & editing, Validation, Supervision, Conceptualization.

Declaration of competing interest

The authors declare that they have no known competing financial interests or personal relationships that could have appeared to influence the work reported in this paper.

Acknowledgments

The authors would like to acknowledge the Federal Ministry of Education and Research (BMBF, Germany) for funding (031B0847A), as well as the Project Management Jülich (PtJ, Germany) for project administration. We thank the ecell Eisenhuth GmbH und Co. KG, Osterode am Harz, Germany, for providing the spheres for the packed bed. We thank the Gescher Lab (Technische Biotechnologie, TUHH, Germany) for providing the inoculum and thank namely Dr. Miriam Edel and Dr. Edina Klein for teaching sterile working techniques. We also thank Axel Heidt and Matthias Weber for their analytical work and help in the lab as well as Alfred Herbst, Erwin Wachter, Joachim Lang and Dennis Happle from the EBI workshop for building the reactor.

Supplementary materials

Supplementary material associated with this article can be found, in the online version, at doi:10.1016/j.rineng.2026.111572.

Data availability

Data will be made available on request.

References

[1] W.-C. Huang and I.-C. Tang, "Chapter 8. Bacterial and yeast cultures-process characteristics, products, and applications," 2007.
[2] A. Schievano, et al., Electro-Fermentation – Merging Electrochemistry With Fermentation in Industrial Applications, Elsevier Ltd, 2016, https://doi.org/10.1016/j.tibtech.2016.04.007. Nov. 01.

[3] S. Ahmad, T. Nawaz, A. Ali, M.F. Orhan, A. Samreen, A.M. Kannan, An Overview of Proton Exchange Membranes For Fuel cells: Materials and Manufacturing, Elsevier Ltd, 2022, https://doi.org/10.1016/j.ijhydene.2022.04.099. May 22.

[4] P. von Tettau, P. Thiele, P. Mauermann, M. Wick, S. Tinz, S. Pischinger, Per- and polyfluoroalkyl Substances in Proton Exchange Membrane Fuel Cells — A review, Elsevier B.V., 2025, https://doi.org/10.1016/j.jpowsour.2024.236104. Feb. 28.

[5] Z. Yang, Y.C. Yong, V. Kumar, Z. Fang, Recent Advances in Electro-Fermentation technology: Sustainable approach For Enhanced Chemical Bioproduction from Mix-Culture to Pure-Culture, Academic Press, 2025, https://doi.org/10.1016/j.jenvman.2025.127895. Dec. 01.

[6] G.K. Rader, B.E. Logan, Multi-electrode continuous flow microbial electrolysis cell for biogas production from acetate, Int. J. Hydrogen Energy 35 (17) (2010) 8848–8854, https://doi.org/10.1016/j.ijhydene.2010.06.033. Sep.

[7] R.D. Cusick, et al., Performance of a pilot-scale continuous flow microbial electrolysis cell fed winery wastewater, Appl. Microbiol. Biotechnol. 89 (6) (2011) 2053–2063, https://doi.org/10.1007/s00253-011-3130-9. Mar.

[8] S. Brunschweiger, et al., The effect of clogging on the long-term stability of different carbon fiber brushes in microbial fuel cells for brewery wastewater treatment, Bioresour. Technol. Rep. 11 (2020), https://doi.org/10.1016/j.biteb.2020.100420. Sep.

[9] M. Hackbarth, J. Gescher, H. Horn, J.E. Reiner, A scalable, rotating disc bioelectrochemical reactor (RDBER) suitable for the cultivation of both cathodic and anodic biofilms, Bioresour. Technol. Rep. 21 (2023), https://doi.org/10.1016/j.biteb.2023.101357. Feb.

[10] M.T. Knoll, N. Jürgensen, J.R. Weiler, J. Gescher, Predictability and robustness of anode biofilm to changing potential in microbial electrolysis system, Bioresour. Technol. Rep. 24 (2023), https://doi.org/10.1016/j.biteb.2023.101640. Dec.

[11] N. Juergensen, J.R. Weiler, M.T. Knoll, J. Gescher, M. Edel, Strategic improvement of *Shewanella oneidensis* for biocatalysis: approach to media refinement and scalable application in a microbial electrochemical system, N. Biotechnol. 85 (2025) 31–38, https://doi.org/10.1016/j.nbt.2024.11.006. Mar.

[12] N.Shylaja Prakash, et al., Evaluation of key operational parameters in a novel pilot-scale rotating disk bioelectrochemical reactor for hydrogen production in a wastewater biorefinery, Chem. Eng. J. 525 (2025), https://doi.org/10.1016/j.cej.2025.168691.

[13] G.F. Froment, K.B. Bischoff, J. De Wilde, The plug flow reactor, Chemical Reactor Analysis and Design (2011) 427–432.

[14] S. Schlegel, H. Koeser, Wastewater treatment with submerged fixed bed biofilm reactor systems - design rules, operating experiences and ongoing developments, Water Sci. Technol. (2007) 83–89, https://doi.org/10.2166/wst.2007.245.

[15] P.V. Danckwerts, Continuous flow systems distribution of residence times, Chem. Eng. Sci. 2 (1) (1953). Feb.

[16] J.M.P.Q. Delgado, Longitudinal and transverse dispersion in porous media, Chem. Eng. Res. Design 85 (9 A) (2007) 1245–1252, https://doi.org/10.1205/cherd07017.

[17] J.R. Quejigo, B. Korth, A. Kuchenbuch, F. Harnisch, Redox potential heterogeneity in fixed-bed electrodes leads to microbial stratification and inhomogeneous performance, ChemSusChem 14 (4) (2021) 1155–1165, https://doi.org/10.1002/cssc.202002611. Feb.

[18] D. Jiang, B. Li, Granular activated carbon single-chamber microbial fuel cells (GAC-SCMFCs): a design suitable for large-scale wastewater treatment processes, Biochem. Eng. J. 47 (1–3) (2009) 31–37, https://doi.org/10.1016/j.bej.2009.06.013. Dec.

[19] S. Wu, et al., A novel pilot-scale stacked microbial fuel cell for efficient electricity generation and wastewater treatment, Water Res. 98 (2016) 396–403, https://doi.org/10.1016/j.watres.2016.04.043. Jul.

[20] S. Ikeda, et al., Shewanella Oneidensis MR-1 As a Bacterial Platform For Electro-Biotechnology, Portland Press Ltd, 2021, https://doi.org/10.1042/EBC20200178. Jul. 01,.

[21] K.H. Nealson, J. Scott, Ecophysiology of the genus *Shewanella*. The Prokaryotes, Springer, New York, 2006, pp. 1133–1151, https://doi.org/10.1007/0-387-30746-x_45.

[22] C. Engel, F. Schattenberg, K. Dohnt, U. Schröder, S. Müller, R. Krull, Long-term behavior of defined mixed cultures of *Geobacter sulfurreducens* and *Shewanella oneidensis* in bioelectrochemical systems, Front. Bioeng. Biotechnol. 7 (2019), https://doi.org/10.3389/fbioe.2019.00060. MAR.

[23] G. Reguera, K.D. McCarthy, T. Mehta, J.S. Nicoll, M.T. Tuominen, D.R. Lovley, Extracellular electron transfer via microbial nanowires, Nature 435 (7045) (2005) 1098–1101, https://doi.org/10.1038/nature03661. Jun.

[24] Y. Cao, et al., A synthetic plasmid toolkit for *Shewanella oneidensis* MR-1, Front. Microbiol. 10 (2019), https://doi.org/10.3389/fmicb.2019.00410. MAR.

[25] T. Bursac, J.A. Gralnick, J. Gescher, Acetoin production via unbalanced fermentation in *Shewanella oneidensis*; Acetoin production via unbalanced fermentation in *Shewanella oneidensis*, Biotechnol. Bioeng. (2017) 1283–1289, https://doi.org/10.1002/bit.26243/abstract.

[26] X. Sun, et al., Construction of *Shewanella oneidensis* chassis for unbalanced fermentation with glycerol by adaptive laboratory evolution, Green Carbon (2025), https://doi.org/10.1016/j.greenca.2025.01.002. Mar.

[27] X. Liu, D.W. Schubert, Influence of the pressure-dependent contact area between electrode and composite surface on the electrical conductivity, Compos. Struct. 136 (2016) 414–418, https://doi.org/10.1016/j.compstruct.2015.10.040. Feb.

[28] A. Hennico, G. Jacques, and T. Vermeulen, "Longitudinal Dispersion in packed extraction columns, University of California, Lawrence Radiation Laboratory Berkeley, California," Mar. 1963.

[29] CAF-Group, "Caroline Ajo-Frankling Research Group, M4 medium recipe," https://cafgroup.lbl.gov/protocols/microbial-electrochemistry/protocolsmicrobial-electrochemistrym4-medium-recipe.

[30] Y.J. Tang, J.S. Hwang, D.E. Wemmer, J.D. Keasling, Shewanella oneidensis MR-1 fluxome under various oxygen conditions, Appl. Environ. Microbiol. 73 (3) (2007) 718–729, https://doi.org/10.1128/AEM.01532-06. Feb.

[31] Y.J. Tang, A.L. Meadows, J.D. Keasling, A kinetic model describing Shewanella oneidensis MR-1 growth, substrate consumption, and product secretion, Biotechnol. Bioeng. 96 (1) (2007) 125–133, https://doi.org/10.1002/bit.21101. Jan.

[32] R.S. Renslow, et al., Modeling substrate utilization, metabolite production, and uranium immobilization in Shewanella Oneidensis biofilms, Front. Environ. Sci. 5 (2017), https://doi.org/10.3389/fenvs.2017.00030. JUN, Jun.

[33] A. Hirose, A. Kouzuma, K. Watanabe, Hydrogen-dependent current generation and energy conservation by Shewanella oneidensis MR-1 in bioelectrochemical systems, J. Biosci. Bioeng. 131 (1) (2021) 27–32, https://doi.org/10.1016/j.jbiosc.2020.08.012. Jan.

[34] C. Liu, Y.A. Gorby, J.M. Zachara, J.K. Fredrickson, C.F. Brown, Reduction kinetics of Fe(III), Co(III), U(VI), Cr(VI), and Tc(VII) in cultures of dissimilatory metal-reducing bacteria, Biotechnol. Bioeng. 80 (6) (2002) 637–649, https://doi.org/10.1002/bit.10430. Dec.

[35] S. Arnon, A.I. Packman, C.G. Peterson, K.A. Gray, Effects of overlying velocity on periphyton structure and denitrification, J. Geophys. Res. Biogeosci. 112 (1) (2007), https://doi.org/10.1029/2006JG000235. Mar.

[36] M. Hackbarth, et al., Monitoring and quantification of bioelectrochemical kyrpidia spormannii biofilm development in a novel flow cell setup, Chem. Eng. J. 390 (2020), https://doi.org/10.1016/j.cej.2020.124604. Jun.

[37] R.C. Wagner, D.F. Call, and B.E. Logan, "Optimal set anode potentials vary in bioelectrochemical systems," Aug. 15, 2010. doi: 10.1021/es101013e.

[38] L. Singh, A.G. Miller, L. Wang, H. Liu, Scaling-up up-flow microbial electrolysis cells with a compact electrode configuration for continuous hydrogen production, Bioresour. Technol. 331 (2021), https://doi.org/10.1016/j.biortech.2021.125030. Jul.

[39] P. Zhu, Y. Zhao, Cyclic voltammetry measurements of electroactive surface area of porous nickel: peak current and peak charge methods and diffusion layer effect, Mater. Chem. Phys. 233 (2019) 60–67, https://doi.org/10.1016/j.matchemphys.2019.05.034. May.